Controllable optical Bloch oscillation in planar graded optical waveguide arrays

M. J. Zheng,[1] J. J. Xiao,[2] and K. W. Yu[1,3,*]

[1]*Department of Physics, The Chinese University of Hong Kong, Shatin, New Territories, Hong Kong, People's Republic of China*

[2]*Department of Electronic and Information Engineering and Key Laboratory of Network Oriented Intelligent Computation, Shenzhen Graduate School, Harbin Institute of Technology, Shenzhen 518055, People's Republic of China*

[3]*Institute of Theoretical Physics, The Chinese University of Hong Kong, Shatin, New Territories, Hong Kong, People's Republic of China*

(Received 4 December 2009; published 17 March 2010)

Optical Bloch oscillation is studied theoretically in planar graded optical waveguide arrays with nearest-neighbor couplings. The gradient in the propagation constants can be achieved with the eletro-optical effect. We identify a variety of normal modes (called gradons) in the waveguide arrays with the aid of a phase diagram. Moreover, the localization properties of the normal modes are characterized and the transitions among these modes are obtained from a picture of overlapping bands. The existence of Bloch oscillation and other oscillations are confirmed by using the field-evolution analysis with various input Gaussian beams. From the results, we obtain a correspondence between gradon localization and Bloch oscillation. This study can be extended to more general waveguide arrays in higher dimensions and with further neighbor couplings. The results offer great potential applications in controlling wave propagation by means of graded materials and graded systems, which can be used to explore the tunability of light manipulation and applied to design suitable optical devices.

DOI: 10.1103/PhysRevA.81.033829 PACS number(s): 42.25.Bs, 42.79.Gn, 42.82.Et, 73.20.Mf

I. INTRODUCTION

Light transferring and processing have become hot topics in modern optics. Artificial materials (e.g., metamaterials [1], photonic crystals [2,3], and waveguide arrays [4]) are used in timely and important studies to manipulate light. Among them, waveguide arrays are simple and promising candidates for realizing the optical analog of electronic Bloch oscillation (BO). BO is the oscillatory motion of a particle in a periodic potential when a constant force is acting on it. The occurrence of BO requires two conditions [5]: (i) periodic potential and (ii) external force. The first condition can be achieved by periodic structures, where Bragg reflection occurs. The second condition can be fulfilled with an external electric field for electronic BOs or linear potential for other BOs of different natures (optical [6], acoustic [7], or matter waves [8]). For optical BOs, optical waveguide arrays with a linear gradient in the propagation constants have been proved to be ideal [6]. The gradient is either a temperature gradient in thermo-optical polymer waveguide arrays [9] or a gradient in a width [10] and/or refractive index [11]. Equivalent linear potential can also be achieved via geometrical variation in waveguides [12–14], for example, helical (deformed) waveguides [12] and curved waveguide arrays [14]. Optical BOs have also been observed in laterally confined structures [15]. The nonlinear [10] and dissipative [16] effects of optical BOs in waveguide arrays have been investigated. Discrete optical solitons have been observed in nonlinear optical waveguide arrays [17]. In two-dimensional waveguide lattices, various types of lattices [18–20], for example, square [18], hexagonal [20], or general lattices [20], have been investigated for optical BOs. Light evolution inside such waveguide arrays is found to be completely determined by the conditions of the input field [19]. However, the correspondence between the dynamic evolution and various input beams has not been fully investigated. In this work, we aim to address such a correspondence in optical waveguide arrays with linearly varying propagation constants.

We have discovered a peculiar kind of localized mode called a gradon in graded elastic lattices whose force constant or mass varies in space [21–25]. We studied gradon physics in one-dimensional graded chains [21,22], two-dimensional orthogonally graded square lattices [23], diagonally graded square lattices [24], and diatomic lattices [25]. The body of research shows that there are a variety of gradon modes and transitions among these modes. Gradon modes have also been identified in various systems, for example, plasmonic gradon modes in graded plasmonic systems [26,27] and photonic gradon modes in graded optical systems [6]. Furthermore, we have discovered an obvious correspondence between plasmonic gradon confinements and various beam oscillations in graded plasmonic waveguides [28].

In this work, we study photonic gradon modes in planar graded optical waveguide arrays (GOWAs). We aim to find the correspondence between various oscillations and confinements of photonic gradon modes in such systems. The eigenmodes are obtained by using an optical-quantum analog method. Various gradon modes are distinguished through a diagrammatic approach. This is based on the band overlapping picture, which is a powerful tool for constructing a phase diagram of a GOWA. The transitions between different localized modes are analyzed through pseudodispersion relation and density of states (DOS). The variety of oscillations in GOWAs is explored using field-evolution analysis, which shows the propagation of a discrete Gaussian beam along the axis of waveguides. It is similar to the wave-packet dynamic analysis used in the graded plasmonic waveguides [28]. The correspondence between these oscillations and gradon confinements can be determined. This study is not only important in understanding the mechanism of BO and non-Bloch oscillation but also useful in photonic applications and engineering functionally graded materials.

*kwyu@phy.cuhk.edu.hk

II. MODEL AND FORMULA

We consider planar GOWAs with a linearly varying propagation constant which can be obtained by taking advantage of the electro-optical effect [6]. As shown in Fig. 1, the waveguide array takes a planar structure composed of individual waveguides, in each of which light propagates along the longitudinal axis of waveguide, that is, the z direction. The waveguide is indexed by n ($n = 1, 2, \ldots, N$). The evanescent fields leaking from nearby waveguides are coupled, leading to a collective supermode. The structure is thus quasi-two-dimensional and the supermodes are laterally (or transversely) confined by the gradon mechanism.

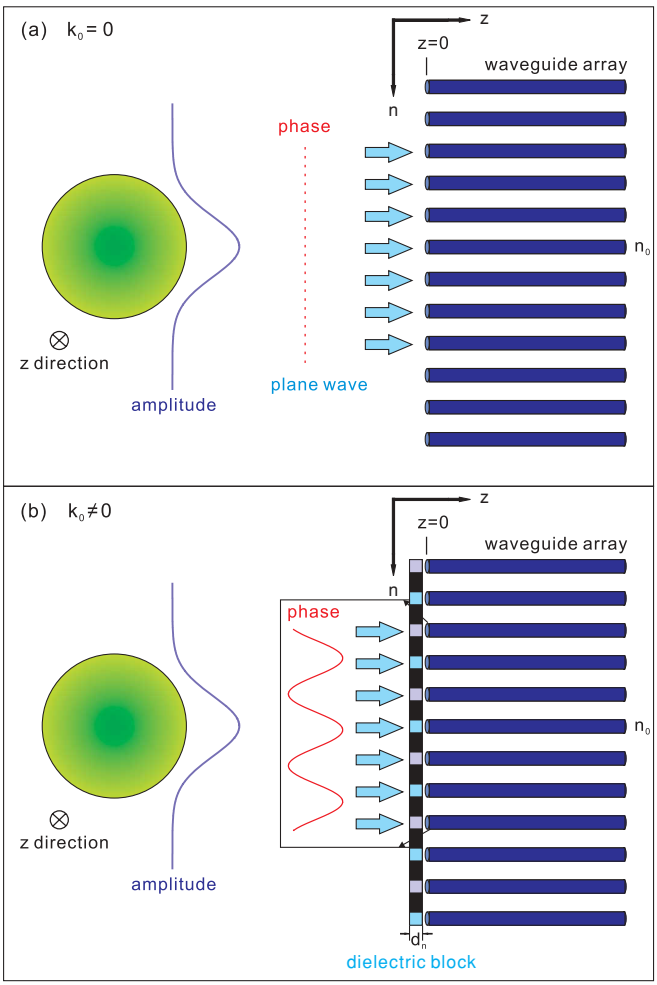

FIG. 1. (Color online) Schematic diagrams for the planar graded optical waveguide arrays and the input Gaussian beam described by Eq. (7), with the input transverse wave numbers (a) $k_0 = 0$ and (b) $k_0 \neq 0$. The light propagates along the axis of the waveguide, i.e., the z direction. The waveguide is labeled as n ($n = 1, 2, \ldots, N$). The graded propagation constant αn varies linearly with n. The boundary conditions of the two cases are as follows: (a) $k_0 = 0$. A plane wave inputs at the $z = 0$ boundary. (b) $k_0 \neq 0$. The additional optical path differences due to the dielectric blocks placed in front of the input channels lead to the required phase differences $\exp[-ik_0(n - n_0)]$ between the nth and n_0th waveguide at the $z = 0$ boundary.

A. Normal-mode approach

According to the coupled-mode theory, the evolutionary equation of modal amplitude a_n in the nth waveguide can be scaled as [6]

$$\left(i\frac{d}{dz} + \alpha n\right) a_n(z) + a_{n+1}(z) + a_{n-1}(z) = 0, \quad (n = 1, 2, \ldots, N), \tag{1}$$

where $\alpha = \Delta/C$ and $z = CZ$ are normalized quantities. Here Δ is the wave-number spacing between two waveguides, C the linear coupling constant, and Z the propagation distance of the beam along the axis of the waveguide. The solution of eigenmodes has the form

$$a_n^m(z) = u_n^m e^{i\beta_m z}, \tag{2}$$

where β_m means the wave number of the supermode m and the transverse mode profile is given by a superposition of the mode amplitudes u_n^m of the individual waveguides. Substituting Eq. (2) into Eq. (1), we have

$$\beta_m u_n^m = \alpha n u_n^m + u_{n+1}^m + u_{n-1}^m. \tag{3}$$

Equation (3) can be written in the matrix form

$$\beta|u\rangle = \mathbf{H}|u\rangle, \tag{4}$$

where the Hamiltonian matrix $\mathbf{H}$ is defined as $H_{nn} = \alpha n$ and $H_{n,n-1} = H_{n,n+1} = 1$. The column vector $|u\rangle$ and β denote the eigenvectors and eigenvalues of $\mathbf{H}$, respectively. In GOWA, these eigenmodes are also called photonic gradon modes.

Using the preceding definition of Hamiltonian matrix $\mathbf{H}$, Eq. (1) can be written as a z-dependent equation:

$$-i\frac{d}{dz}|u\rangle = \mathbf{H}|u\rangle. \tag{5}$$

It is analogous to the Schrödinger equation in quantum system,

$$i\frac{d}{dt}|\phi\rangle = \mathbf{H}|\phi\rangle. \tag{6}$$

Here $\hbar$ is taken to be unity. We note that z and β in GOWAs are equivalent to t and ω in a quantum system, respectively.

B. Field-evolution analysis

In this study, we perform the field-evolution analysis with the input wave function at $z = 0$,

$$\psi(0) = \frac{1}{(2\pi\sigma^2)^{1/4}} e^{-\frac{(n-n_0)^2}{4\sigma^2}} e^{-ik_0(n-n_0)}, \tag{7}$$

where k_0 is the input transverse wave number. The incoming field at z ($z < 0$) is $\psi(z) = \psi(0)\exp(i\beta_0 z)$, where β_0 is the propagation constant of an individual channel. The intensity profile $|\psi(0)|^2$ has a discrete Gaussian distribution centered at the n_0th waveguide with spatial width σ. This kind of input beam is referred to as a discrete Gaussian beam. The exponential factor $\exp[-ik_0(n - n_0)]$ denotes the phase differences between input beams excited on the nth and the n_0th waveguides. We note that $k_0 = 0$ represents the case where the phase difference between input beams at different waveguides is zero; that is, the input beam is a plane wave, as shown in Fig. 1(a). Finite phase differences are realized by putting some small blocks of dielectric mediums with different

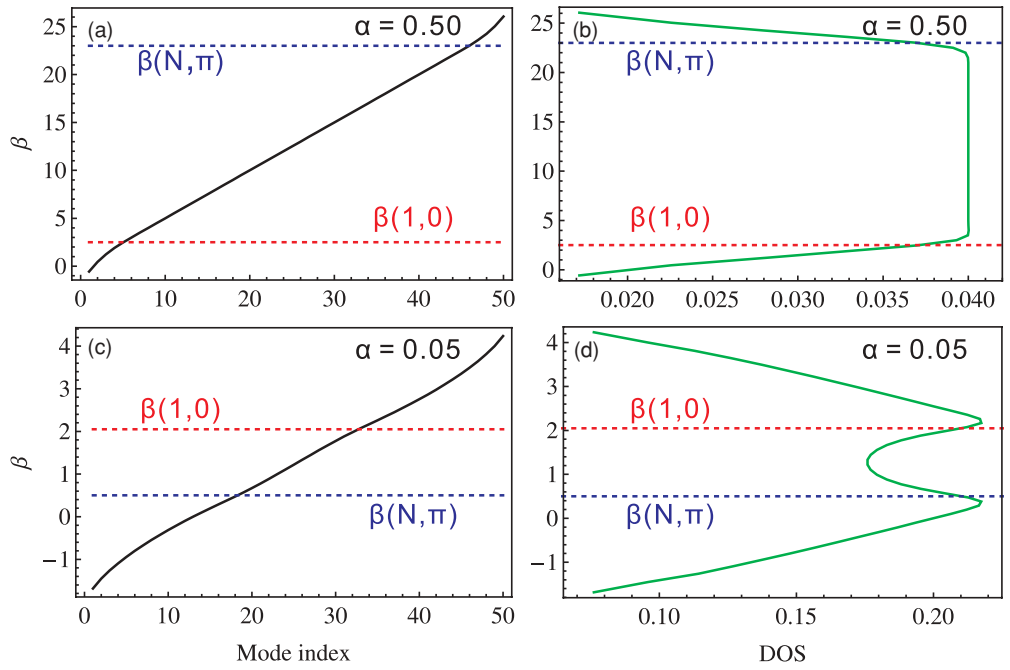

FIG. 2. (Color online) Pseudodispersion relation between β and the supermode index number m for (a) $\alpha = 0.5$ when $\beta(N,\pi) > \beta(1,0)$ and (c) $\alpha = 0.05$ when $\beta(N,\pi) < \beta(1,0)$. Panels (b) and (d) are the corresponding density of states (DOS) for (a) and (c), respectively.

thicknesses or refractive index right in front of each waveguide, as shown in Fig. 1(b). The additional optical path differences due to the dielectric blocks placed in front of the input channels lead to the required phase differences and set up a finite k_0 in the input discrete Gaussian beam.

We can expand the input wave function in terms of the supermodes $|u_m\rangle$,

$$|\psi(0)\rangle = \sum_m A_m |u_m\rangle, \tag{8}$$

where $A_m = \langle u_m|\psi(0)\rangle$ is the constituent component of the input Gaussian beam. The subsequent wave function at propagation distance z is

$$|\psi(z)\rangle = \sum_m A_m e^{i\beta_m z}|u_m\rangle. \tag{9}$$

The evolution of beam intensity $|\psi(z)|^2$ along the propagation distance z is used to illustrate various oscillations, including BO, breathing-wave-like (BW) oscillation, and other kinds of motions.

The gradon dynamics can also be calculated with the approach of Hamiltonian optics. The evolution of a beam can be obtained by solving the Hamiltonian for the mean values of position $\langle x\rangle$ and wave vector $\langle k\rangle$. However, the Hamiltonian optics approach cannot reveal the width of the field evolution.

III. PHOTONIC GRADON MODES IN PLANAR GRADED OPTICAL WAVEGUIDE ARRAYS

The photonic gradon modes are obtained by directly diagonalizing the eigenvalue problem of GOWAs, as described by Eq. (4). Since the variables (β, z) in the optical waveguide arrays correspond to (ω, t) in a quantum system, we refer to the functional dependence of β on the transverse wave number k as the dispersion relation in periodic optical waveguide arrays. In GOWAs, although the broken translational symmetry in the gradient direction does not allow us to consider such a dispersion relation, the relationship between the eigenvalue β and the mode index m, which is defined as the ascending order with respect to β_m, can be regarded as a pseudodispersion relation [23], as shown in Figs. 2(a) and 2(c) for $\alpha = 0.50$ and $\alpha = 0.05$, respectively. Figures 2(b) and 2(d) are the corresponding numerical DOS, which describe the number of states per unit β. These numerical DOS are obtained by $D(\beta) = 1/(N\partial\beta/\partial m)$. To understand the pseudodispersion relation, we divide the infinite graded waveguide array into a large number of subwaveguide arrays, each of which is still infinite in size. Because the gradient in each subwaveguide array is infinitesimal, we can treat it as homogeneous; thus, the solution satisfies the relation $u_{n+1} = u_n \exp(ik)$, where k is the transverse wave vector. Substituting this relation into Eq. (3), we obtain the analytic local dispersion relation

$$\beta(n,k) = \alpha n + 2\cos k \tag{10}$$

for a subwaveguide array with a specific propagation constant αn. Here the mode index m is omitted for simplicity. For various propagation constants αn $(n = 1, 2, \ldots, N)$, two overlapping bands are obtained by $\beta(n,0) = \alpha n + 2$ and $\beta(n,\pi) = \alpha n - 2$. With the aid of a band-overlapping picture, the phase diagram is constructed as shown in Fig. 3. The lower and upper limits of the two bands determine the four phase boundaries in the phase diagram: $\beta(1,\pi) = \alpha - 2$ (solid line), $\beta(1,0) = \alpha + 2$ (dotted line), $\beta(N,\pi) = \alpha N - 2$ (dash-dotted line), and $\beta(N,0) = \alpha N + 2$ (dashed line). The intersections of the four lines define the four phase regions, each of which corresponds to a particular kind of photonic gradon mode. Different kinds of modes are

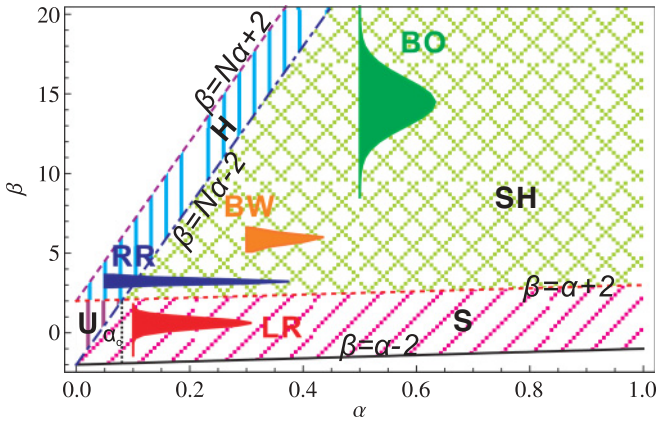

FIG. 3. (Color online) Phase diagram for the planar graded optical waveguide arrays with $N = 50$ waveguides. There are four regions of different gradon modes in the phase diagram as follows: soft gradon (S), hard gradon (H), soft-hard gradon (SH), and unbounded modes (U). The corresponding oscillations for input beams consist of different gradon modes are as follows: LR, left-end reflection; RR, right-end reflection; BW, breathing-wave-like oscillations; BO, Bloch oscillation. The left-and-right-end reflection (LRR) in the U region is not shown here. The distribution of a component for each kind of oscillation is marked on the corresponding positions on the phase diagram.

localized at different transverse positions of the waveguide arrays. When $\beta(n,0) = \beta(n,\pi)$, that is, $\alpha + 2 = \alpha N - 2$, the critical value $\alpha_c = 4/(N-1)$ is obtained. For $\alpha < \alpha_c$, the unbound (extended) modes (U) cover a wave-number range $\alpha N - 2 < \beta < \alpha + 2$ (lower vertical-line-shaded region). In the lower wavenumber range $\alpha - 2 < \beta < \alpha N - 2$ (when $\alpha < \alpha_c$) and $\alpha - 2 < \beta < \alpha + 2$ (when $\alpha > \alpha_c$), the modes are localized at the left-hand side of the array, and are called soft photonic gradons (S) (slanted-dotted-line-shaded region). In the higher wave-number range $\alpha + 2 < \beta < \alpha N + 2$ (when $\alpha < \alpha_c$) and $\alpha N - 2 < \beta < \alpha N + 2$ (when $\alpha > \alpha_c$), the modes are localized at the right-hand side of the array and are called hard photonic gradons (H) (upper vertical-line-shaded region). The gradon modes in GOWAs can be characterized by a mapping of the dynamic equation Eq. (1) to that of a spring-mass chain with graded force constants [21,23]. The force constant is smaller (larger) at the left (right) side of the chain, and thus the modes localized at the left (right) side are called soft (hard) gradons. For $\alpha > \alpha_c$, the modes become localized in the middle parts of the array and cover a wave-number range $\alpha + 2 < \beta < \alpha N - 2$ (cross-hatched region). We call these modes soft-hard photonic gradons (SH). The mode patterns of typical photonic gradon modes, that is, the numerical modal amplitude versus waveguide index, are demonstrated in Fig. 4. Figures 4(a) and 4(b) are mode patterns of SH with different eigenvalues of β. They are localized in the middle part of the waveguide array. The numerical results are similar to the analytic results in the Ref. [6]. Figures 4(c) and 4(d) are mode patterns of S and H, which are localized at the left and right parts of the waveguide array, respectively.

At the phase boundaries, transitions between different localized gradon modes occur. A critical wave number is referred to as the transition wave number. For example, the transition wave numbers $\beta(1,0) = \alpha + 2$ and $\beta(N,\pi) = \alpha N - 2$ are marked on the plots of pseudodispersion relation and DOS, as shown in Fig. 2. Here two specific values of α are chosen, one for $\alpha = 0.50$ when SH exists and the other for $\alpha = 0.05$ when no SH exists. For $\alpha = 0.50$ ($\alpha > \alpha_c$), as shown in Figs. 2(a) and 2(b), $\beta(1,0) < \beta(N,\pi)$, SH exists in the intermediate wave-number range $\beta(1,0) < \beta < \beta(N,\pi)$. Thus, at $\beta(1,0)$, S-SH transition occurs, and at $\beta(N,\pi)$, SH-H transition takes place. It is evident that DOS is almost

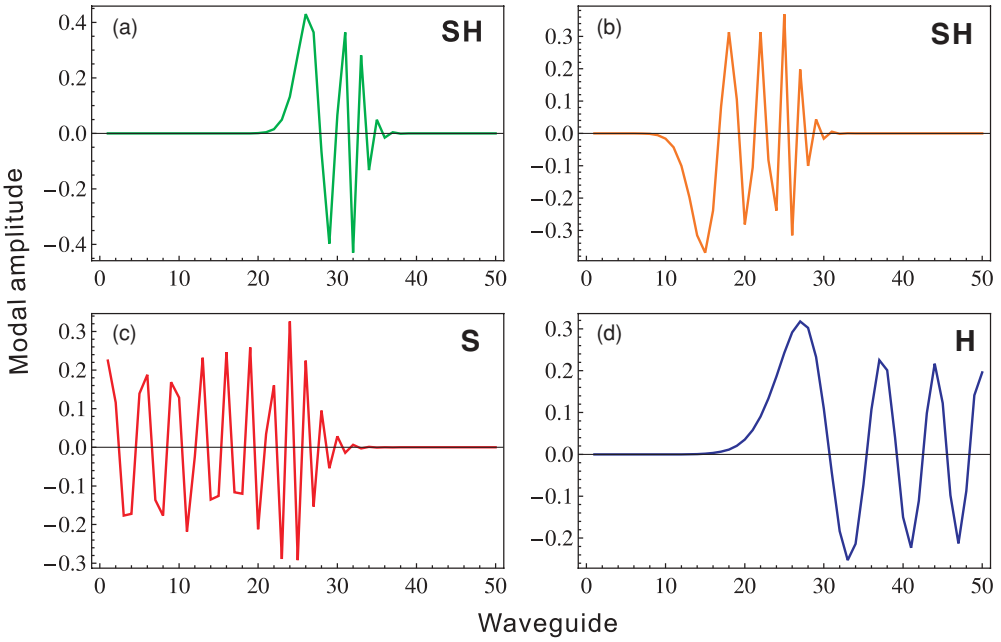

FIG. 4. (Color online) Typical mode patterns of (a) and (b) soft-hard gradon (SH), (c) soft gradon (S), and (d) hard gradon (H), corresponding to the dominant modes of beams, which undergo Bloch oscillation, breathing-wave-like oscillation, left-end reflection, and right-end reflection, respectively. The unit of the model amplitude is arbitrary, while the abscissa denotes the waveguide index.

constant for SH. These modes with equal energy distance are commonly referred to as Wannier-Stark states (WSSs) in Ref. [6]. For $\alpha = 0.05$ ($\alpha < \alpha_c$), $\beta(1,0) > \beta(N,\pi)$ as shown in Figs. 2(c) and 2(d), no SH exists and only unbounded modes survive in the intermediate wave-number range $\beta(N,\pi) < \beta < \beta(1,0)$. Thus, at $\beta(N,\pi)$, the S-U transition happens, and at $\beta(1,0)$, the U-H transition occurs. The DOS is not flat for unbounded modes, which are different from WSSs. These transitions between various gradon modes indicate that it is possible to vary the localized position and extension of photonic gradon modes. Furthermore, the types of transition are controllable for different gradients α. It offers more options to realize light manipulation by varying gradients. To achieve tunability, it is quite necessary to understand the correspondence between different localized gradon modes and evolutions of light beams in these planar GOWAs.

IV. CORRESPONDENCE BETWEEN VARIOUS OSCILLATIONS AND GRADON CONFINEMENTS

Here a few cases are addressed to illustrate the correspondence between the gradon confinements and the various oscillations of incoming beams. The occurrence of various oscillations depends on the localization extent of modes forming the input beams. Since the phase diagram as sketched in Fig. 3 explicitly reflects the spatial extension of the various gradon modes that the planar GOWAs sustain, it helps us to have an instant judgment about whether an input beam contains a component that can reach either the left or the right end of the array, where reflection by the boundary occurs. Such beams shall not undergo BO or BW oscillation. A necessary condition for the occurrence of BO or BW oscillation is that the input beam only consists of soft-hard gradons, because SH are localized in the middle part of the array. We have marked the constituent components ($|A_m|^2$ versus β) of the different input beams at certain α on the phase diagram (see Fig. 3). As expected, in the SH region, BO can occur. Depending on the input beam, BW oscillations can also occur. The differences are that the input beam for BO has a larger spatial width than that for BW. In the S region, the input beam consisting of soft gradons is reflected at the left end of the array, such a dynamic evolution is denoted by LR (left-end reflection). While in the H region, right-end reflection, denoted by RR, occurs. Finally, in the U region, an extended beam can be reflected by both

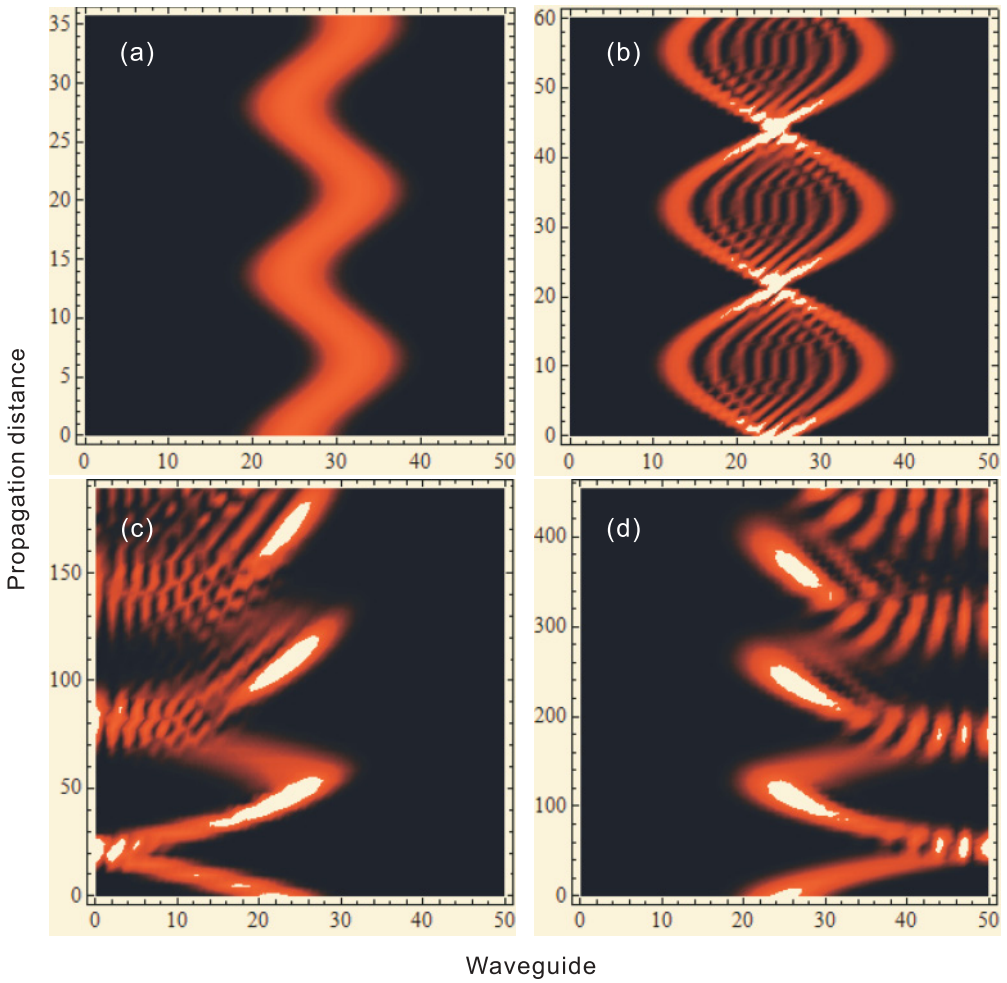

FIG. 5. (Color online) Evolution of various excitation beams shown by the contour plots of $|\psi(z)|^2$ on the propagation distance-waveguide domain. The rescaled propagation distance is dimensionless, while the abscissa denotes the waveguide index. (a) Bloch oscillation ($\alpha = 0.5$, $\sigma = 3, k = 0.0$), (b) breathing-wave-like oscillation ($\alpha = 0.3, \sigma = 0.02, k = 0.8\pi$), (c) reflection from the left end ($\alpha = 0.1, \sigma = 3, k = 0.9\pi$), and (d) reflection from the right end ($\alpha = 0.05$, $\sigma = 3$, $k = 0.0$).

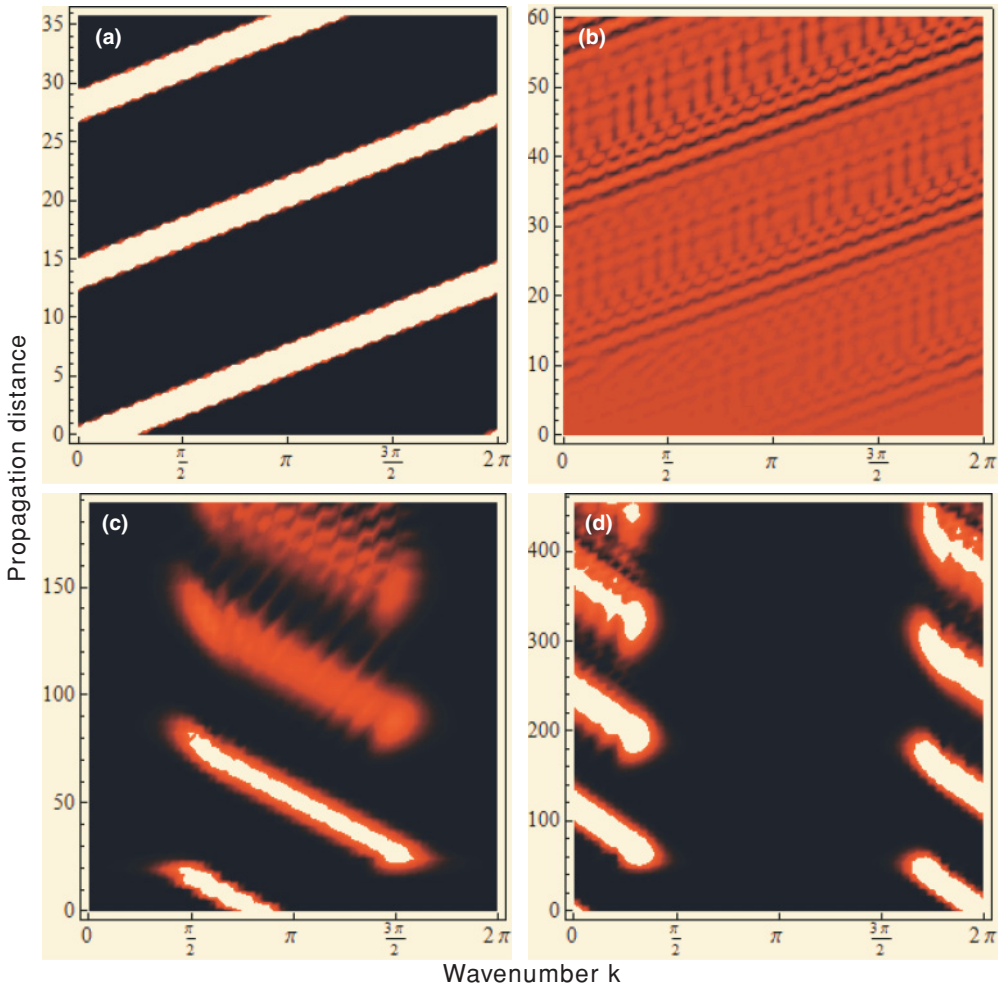

FIG. 6. (Color online) Evolution of various excitation beams in k-space shown by the contour plots of $|\phi(k)|^2$ in the reciprocal position-propagation distance (i.e., k-z) domain. The rescaled propagation distance is dimensionless. (a) Bloch oscillation ($\alpha = 0.5, \sigma = 3, k = 0.0$), (b) breathing-wave-like oscillation ($\alpha = 0.3, \sigma = 0.02, k = 0.8\pi$), (c) reflection from the left end ($\alpha = 0.1, \sigma = 3, k = 0.9\pi$), and (d) reflection from the right end ($\alpha = 0.05, \sigma = 3, k = 0.0$).

ends of the array, which is denoted by LRR (left-and-right-end reflection), though it is not marked on the phase diagram.

These various oscillations are clearly observed from the contour plots of $|\psi(z)|^2$ in the β-α domain, as shown in Fig. 5. The bright and intermediate regions indicate the very strong and relatively strong intensity, respectively, and the dark region is where the intensity is weak or zero. Figure 5(a) shows the evolution of $|\psi(z)|^2$ for $\alpha = 0.5$, $\sigma = 3$, and $k_0 = 0.0$. The beam exhibits an oscillatory motion: the mean position shows a periodic oscillation while the width is nearly constant. This is a typical optical BO process. In Fig. 5(b), we show the case of $\alpha = 0.3$, $\sigma = 0.02$, and $k_0 = 0.8\pi$. Now the beam's width shows a periodic variation but the mean position is nearly fixed at the central input waveguide. This is a BW oscillation. Both input beams for BO and BW oscillation are only formed by soft-hard gradons, which are normal modes localized in the middle part of the system. The difference is that the width of input beam for BO ($\sigma = 3$) is much wider than that for BW oscillation ($\sigma = 0.02$).

The different features of BO and BW oscillation are also demonstrated in the contour plots of $|\phi(k)|^2$ in the wave-number-propagation distance (i.e., k-z) domain, as shown in Figs. 6(a) and 6(b). The reciprocal space wave function $\phi(k)$ is obtained from the Fourier transform of the real-space wave function $\psi(x)$. The bright and intermediate regions indicate the very strong and relatively strong intensity, respectively, and the dark region is where the intensity is weak or zero. The intensity $|\phi(k)|^2$ varies periodically in the range $[0, 2\pi]$. Since we assumed a minimum uncertainty input beam, a large (small) spatial x width for BO (BW) leads to a small (large) momentum k width for BO (BW).

Besides the BO and BW oscillations, there are some other oscillations, for example, reflection from the left end, the right end, or both ends. Figure 5(c) ($\alpha = 0.1$, $\sigma = 3$, $k_0 = 0.9\pi$) shows the reflection from the left end. In this case, the input beam only consists of soft gradons, which are localized at the left end of the system. Figure 5(d) ($\alpha = 0.05, \sigma = 3, k_0 = 0.0$) demonstrates the right reflection for input beams formed by hard gradons. The corresponding evolutions in k space are shown in Fig. 6(c) and 6(d), respectively. If the components of an input beam all fall into the extended mode (U) region, the beam can reach both ends and be reflected in multiple fashions

before eventually spreading across the whole waveguide array (contour plot not shown here).

V. DISCUSSION AND CONCLUSION

Understanding the correspondence between various beam oscillations and gradon confinements, we propose a mechanism for controlling light in optical waveguide arrays. The correspondence lies in that the BO period and its spatial range of oscillation depend on the gradient. The results may permit implementation in electro-optical switching or steering devices. Thus, by changing the applied voltage across the waveguide arrays, the output channel can be varied in a controlled way. Similarly, we can take advantage of the thermo-optical effect to achieve optical switching.

We can extend our study to diatomic and higher-dimensional planar GOWAs. The gradient may have different settings or be directed along different directions with respect to the lattices. We can further introduce a single impurity to the GOWA and study the localized modes due to the defect. It is also interesting to explore the correspondence between gradon confinements and slow light, which can be analyzed with a hybridization model [29].

In summary, we study the optical BOs in planar GOWAs with nearest-neighbor couplings. A variety of photonic gradon modes are obtained: soft gradons, hard gradons, soft-hard gradons, and unbounded modes. Excitation beams consisting of different types of gradon modes undergo different evolutionary oscillations. The correspondences between various oscillations and gradon confinements have been established through a phase diagram, which is constructed via a band-overlapping picture. The understanding of such correspondence would have important applications in both photonics and functional materials.

ACKNOWLEDGMENTS

This work was supported by RGC General Research Fund of the Hong Kong SAR Government. We thank Kousuke Yakubo for careful reading of the manuscript and for many useful discussion and helpful suggestions.

[1] D. R. Smith, J. B. Pendry, and M. C. K. Wiltshire, Science **305**, 788 (2004).
[2] M. Notomi, Phys. Rev. B **62**, 10696 (2000).
[3] G. von Freymann, W. Koch, D. C. Meisel, M. Wegener, M. Diem, A. Garcia-Martin, S. Pereira, K. Busch, J. Schilling, R. B. Wehrspohn, and U. Gosele, Appl. Phys. Lett. **83**, 614 (2003).
[4] H. Trompeter, Discrete Optics in Inhomogeneous Waveguide Arrays, Ph.D. dissertation, Friedrich-Schiller Universitat Jena, 2006.
[5] T. Hartmann, F. Keck, H. J. Korsch, and S. Mossmann, New J. Phys. **6**, 2 (2004).
[6] U. Peschel, T. Pertsch, and F. Lederer, Opt. Lett. **23**, 1701 (1998).
[7] H. Sanchis-Alepuz, Y. A. Kosevich, and J. Sanchez-Dehesa, Phys. Rev. Lett. **98**, 134301 (2007).
[8] B. M. Breid, D. Witthaut, and H. J. Korsch, New J. Phys. **9**, 62 (2007).
[9] T. Pertsch, P. Dannberg, W. Elflein, A. Bräuer, and F. Lederer, Phys. Rev. Lett. **83**, 4752 (1999).
[10] R. Morandotti, U. Peschel, J. S. Aitchison, H. S. Eisenberg, and Y. Silberberg, Phys. Rev. Lett. **83**, 4756 (1999).
[11] R. Sapienza, P. Costantino, and D. Wiersma, M. Ghulinyan, C. J. Oton, and L. Pavesi, Phys. Rev. Lett. **91**, 263902 (2003).
[12] S. Longhi, Phys. Rev. B **76**, 195119 (2007).
[13] S. Longhi, Opt. Lett. **32**, 2647 (2007).
[14] G. Lenz, I. Talanina, and C. M. de Sterke, Phys. Rev. Lett. **83**, 963 (1999).
[15] A. Kavokin, G. Malpuech, A. Di Carlo, P. Lugli, and F. Rossi, Phys. Rev. B **61**, 4413 (2000).
[16] N. K. Efremidis and D. N. Christodoulides, Opt. Lett. **29**, 2485 (2004).
[17] F. Lederer, G. I. Stegemanb, D. N. Christodoulides, G. Assanto, M. Segev, and Y. Silberberg, Phys. Rep. **463**, 1 (2008).
[18] H. Trompeter, W. Krolikowski, D. N. Neshev, A. S. Desyatnikov, A. A. Sukhorukov, Y. S. Kivshar, T. Pertsch, U. Peschel, and F. Lederer, Phys. Rev. Lett. **96**, 053903 (2006).
[19] A. Szameit, T. Pertsch, F. Dreisow, S. Nolte, A. Tunnermann, U. Peschel, and F. Lederer, Phys. Rev. A **75**, 053814 (2007).
[20] A. Szameit, T. Pertsch, S. Nolte, A. Tunnermann, U. Peschel, and F. Lederer, J. Opt. Soc. Am. B **24**, 2632 (2007).
[21] J. J. Xiao, K. Yakubo, and K. W. Yu, Phys. Rev. B **73**, 054201 (2006).
[22] K. Yakubo, J. J. Xiao, and K. W. Yu, Physica B **394**, 262 (2007).
[23] J. J. Xiao, K. Yakubo, and K. W. Yu, Phys. Rev. B **73**, 224201 (2006).
[24] J. J. Xiao, K. Yakubo, and K. W. Yu, J. Phys. Soc. Jpn. **76**, 024602 (2007).
[25] J. J. Xiao, K. Yakubo, and K. W. Yu, J. Phys. Condens. Matter **19**, 026224 (2007).
[26] J. J. Xiao, K. Yakubo, and K. W. Yu, Appl. Phys. Lett. **88**, 241111 (2006).
[27] J. J. Xiao, K. Yakubo, and K. W. Yu, Appl. Phys. Lett. **89**, 221503 (2006).
[28] M. J. Zheng, J. J. Xiao, and K. W. Yu, J. Appl. Phys. **106**, 113307 (2009).
[29] C. W. Ling, M. J. Zheng, and K. W. Yu, Opt. Commun. **283**, 1945 (2010).